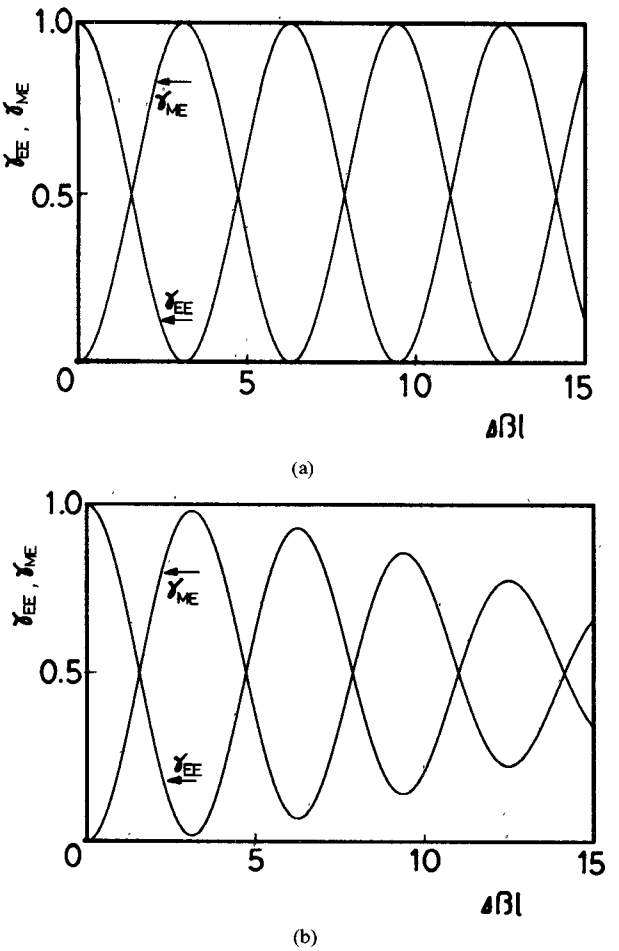

Fig. 3. TE–TM mode conversion efficiency for (a) linearly polarized hybrid modes and (b) circularly polarized hybrid modes.

for $0 < z < l$. The wavelength in vacuum is $\lambda_0 = 1.15\ \mu$m, and the film thickness[2] is $d_0 = .2262\lambda_0$. The hybrid modes are circularly polarized because we have anisotropic polar configuration in this case. Then, the hybrid mode beam waves propagate as shown in Fig. 2(b) ($\tan\theta^+ = +0.001475$, $\tan\theta^- = -0.001643$). The conversion efficiency is shown in Fig. 3(b), where the beam width is $W = 50\ \mu$m.

In the case of pure imaginary[3] ϵ_{23} (i.e., gyrotropic polar case), the hybrid modes have linear polarizations perpendicular to each other. Then, $\theta^+ = 0$ and $\theta^- = 0$. The propagation path of the beam waves and the conversion efficiency are shown in Fig. 2(a) and Fig. 3(a), respectively. Complete TE–TM mode conversion is available at $\Delta\beta l = (2n-1)\pi$, $n = 1, 2, \cdots$.

III. Conclusions

We have given TE–TM mode conversion efficiency when a Gaussian beam wave propagates in thin-film optical waveguide with uniaxial anisotropic substrates. It should be noted that the direction of power flow of hybrid modes depends on the polarization when the TE–TM mode conversion is described as coupling between the two hybrid modes. For efficient TE–TM mode conversion, it is desirable that the uniaxial anisotropic substrates have a configuration sufficient to produce the linearly polarized hybrid modes, i.e., anisotropic longitudinal and gyrotropic polar configurations. The property of oblique power flow of the hybrid modes may be useful for thin-film waveguide-type optical deflectors and optical power dividers.

[2] In this example the confinement of the optical field in the guiding region may not be very strong. The conversion efficiencies of Fig. 3 are approximate ones.

[3] The ϵ_{ij}'s of dielectric tensor are real for the rotation of the optic axis of dielectric crystals, but here imaginary ϵ_{ij} is introduced to stand for gyrotropic media. For the direction of external magnetic field in the case of gyrotropic media, see [1, fig. 2].

References

[1] S. Wang, J. D. Crow, and M. Shah, "Studies of the use of gyrotropic and anisotropic materials for mode conversion in thin-film optical waveguide applications," *J. Appl. Phys.*, vol. 43, pp. 1861–1875, Apr. 1972.

[2] S. Wang, J. D Crow, S. L. Wong, and M. Shah, "Eigen mode analysis of wave propagation in optical waveguides deposited on gyrotropic and anisotropic substrates," *J. Appl. Phys.*, vol. 44, pp. 3232–3239, Jul. 1973.

[3] S Yamamoto, Y. Koyamada, and T. Makimoto, "Normal-mode analysis of anisotropic and gyrotropic thin-film waveguides for integrated optics," *J. Appl. Phys.*, vol. 43, pp. 5090–5097, Dec 1972.

[4] J. Warner, "Faraday optical isorator/gyrator design in planar dielectric waveguide form," *IEEE Trans. Microwave Theory Tech.*, vol. MMT-21, pp. 769–775, Dec. 1973.

[5] V. K. Agrawal, Y. Miyazaki, and Y. Akao, "Waveguide type optical modulator using Kerr magnetooptic effects in Ni–Fe thin-films: Theoretical study," *Japan. J. Appl. Phys.*, vol. 15, pp. 2155–2171, Nov 1976.

[6] K. Taki, Y. Miyazaki, and Y. Akao, "Optical propagation and conversion properties of hybrid modes in YIG thin-film waveguides on GGG substrates using Faraday effects with isotropic top layers," *Trans. IECE Japan*, vol. E63, pp. 754–761, Oct. 1980.

[7] W. K. Burns and J. Warner, "Mode dispersion in uniaxial optical waveguides," *J. Opt. Soc. Amer.*, vol. 64, pp. 441–446, Apr. 1974.

[8] D. D. Gia Russo and J. H. Harris, "Wave propagation in anisotropic thin-film optical waveguides," *J. Opt. Soc. Amer.*, vol. 63, pp. 138–145, Feb. 1973.

[9] M. S. Kharusi, "Uniaxial and biaxial anisotropy in thin-film optical waveguides," *J. Opt. Soc. Amer.*, vol. 64, pp. 27–35, Jan. 1974.

[10] H. L. Bertoni and A. Hessel, "Surface waves on a uniaxial plasma slab —Their group velocity and power flow," *IEEE Trans. Antennas Propagat.*, vol. AP-14, pp 352–359, May 1966.

[11] K. Hano, "Zig-zag ray model of hybrid modes in thin-film optical waveguides with uniaxial anisotropic substrates," *J. Opt. Soc. Amer. A*, vol. 4, pp. 1887–1894, Oct. 1987.

[12] Y. Suematsu, "Tunable parametric oscillator using a guided wave structure," *Japan. J. Appl. Phys.*, vol. 9, pp. 798–805, Jul. 1970.

[13] M. Izutsu and T. Sueta, "Optical parametric interactions in dielectric waveguide," *Trans. IECE Japan*, vol. 56-C, pp. 623–630, Dec. 1973.

[14] M. J. Adams, *An Introduction to Optical Waveguides*. New York: Wiley, 1981.

Two-Layer Dielectric Microstrip Line Structure: SiO_2 on Si and GaAs on Si: Modeling and Measurement

R. A. LAWTON, SENIOR MEMBER, IEEE, AND
WALLACE T. ANDERSON, MEMBER, IEEE

***Abstract*—Further development is reported of the modeling of the two-layer dielectric microstrip line structure by computing the scattering parameter S_{21} derived from the model and comparing the computed value with the measured value over the frequency range from 90 MHz to 18 GHz. The sensitivity of the phase of S_{21} and the magnitude of the characteristic impedance to various parameters of the equivalent circuit is**

Manuscript received June 25, 1987; revised October 30, 1987.

R. A. Lawton was with the National Bureau of Standards, Boulder, CO. He is now with Boulder Research Associates, Boulder, CO 80303.

W. T. Anderson is with the Naval Research Laboratory, Washington, DC 20375.

IEEE Log Number 8719443.

also discussed. Examples are given of the measurement and modeling of the SiO_2 on silicon system to 18 GHz and the modeling of the GaAs on silicon system to 100 GHz.

I. Introduction

The two-layer dielectric microstrip line structure is a structure that has found use in a number of applications. Two examples are as follows: In [1] the two-layer structure is used to make a pulse waveform filter with useful characteristics, while in [2] one layer (a silicon layer) is used to provide a high-quality substrate for gallium arsenide devices.

To further amplify the application described in [2], the advantages of integrating GaAs devices on Si substrates include the possibilities of GaAs monolithic microwave integrated circuits (MMIC's) and/or GaAs digital IC's with Si VLSI, electro-optical GaAs devices with Si VLSI, GaAs power FET's on Si substrates for operation above 10 GHz making use of the higher thermal conductivity of Si, and allowing GaAs IC's to be fabricated on much larger diameter Si substrates (> 7.5 cm) than are now available for GaAs. Well-behaved GaAs MESFET's [4] and bipolar transistors [5] have been fabricated on GaAs molecular beam epitaxy (MBE) layers grown on Si. For low-loss applications, methods have been developed to grow high-resistivity GaAs layers on Si by low-temperature MBE (104 $\Omega\cdot$cm) [6] and by V-doped metal-organic chemical vapor deposition (MOCVD) (10^8 $\Omega\cdot$cm) [7].

Preliminary modeling of microstrip lines made from such structures has been described [1], [8]–[10]. Similar analyses have been developed for the increasingly important coplanar waveguide case [11]. In the previous work by Lawton *et al.* [1], the equivalent circuit relations developed by Hasegawa [8] were used to calculate an approximate relation for the microstrip line characteristic impedance and the transition duration of the microstrip line to a step input signal. This approximate relation was then compared with values determined experimentally. In this report, the complete equations for the characteristic impedance and propagation constant of the stripline are developed, including planar skin effect, and used in the calculations without the approximations of [1]. A measurement is then made of the S parameters of the stripline on an automatic network analyzer. In the process, an algorithm is used which transforms the data to the time domain and sets a time window which discards data due to the connectors, so that one is left with data due to the semiconductor stripline itself. The data are then transformed back to the frequency domain.

II. Theory

The structure of the two-layer dielectric transmission system is shown in Fig. 1. A more generalized form of the equivalent circuit will be used here than that of Hasegawa [8] and Lawton *et al.* [1]. This more general equivalent circuit will allow for loss in both dielectric layers and skin effect in the metallization. This equivalent circuit is shown in Fig. 2. Therefore the series impedance is given by

$$Z(j\omega) = j\omega L + R + k\sqrt{j\omega} \tag{1}$$

and the shunt admittance is given by

$$Y(j\omega) = \frac{1}{\dfrac{1}{G_1 + j\omega C_1} + \dfrac{1}{G_2 + j\omega C_2}} \tag{2}$$

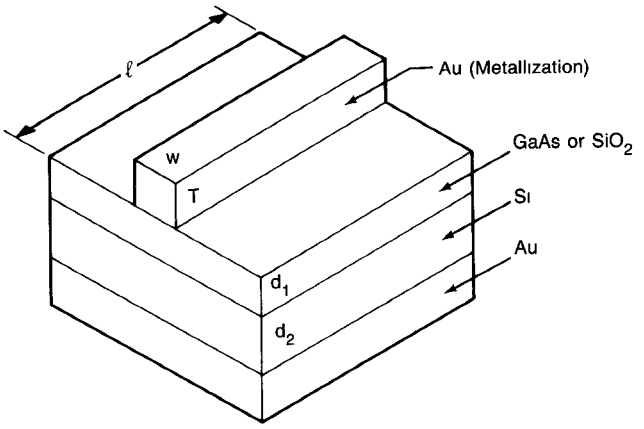

Fig. 1. Two-layer dielectric transmission system.

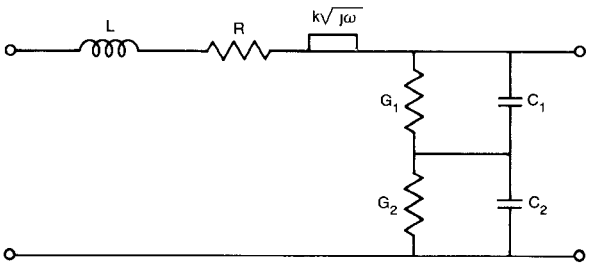

Fig. 2. Generalized two-layer dielectric equivalent circuit.

where

$$R = 1/(\sigma_{Au} wT)$$
$$L = \mu_0 (d_1 + d_2)^+ / w$$
$$C_1 = \epsilon_0 \epsilon_1^+ w/d_1^+$$
$$G_1 = \sigma_1^+ w/d_1^+$$
$$C_2 = \epsilon_0 \epsilon_2^+ w/d_2^+$$
$$G_2 = \sigma_2^+ w/d_2^+$$
$$\omega = \text{angular frequency.}$$

The term $k\sqrt{j\omega}$ represents an impedance term due to planar skin effect. The terms μ and ϵ represent permeability and permittivity, respectively, with the subscripts denoting the medium (0 denotes free space). The other parameters are as defined in Fig. 1. The + superscript denotes effective values that take into account fringing and a mixed dielectric. The defining relations for these effective values are given in [1] and [3].

With the above parameters in (1) and (2), one can calculate the series impedance and shunt admittance elements. One can then substitute (1) and (2) into the expressions for the characteristic impedance:

$$Z_0(j\omega) = \sqrt{Z(j\omega)/Y(j\omega)} \tag{3}$$

and the propagation constant:

$$\gamma(j\omega) = \sqrt{Z(j\omega)Y(j\omega)}\,. \tag{4}$$

These are the parameters which are required to evaluate the behavior of the stripline with a microwave measurement system. However since most modern microwave measurements are made in terms of S parameters, it is desirable to make the further calculation

$$S_{21}(j\omega) = e^{-\gamma(j\omega)l}. \tag{5}$$

This expression is valid for the transmission between two reference planes on a uniform transmission line, which is the case in Fig. 1. The phase of S_{21} is given by the imaginary part of the exponent and the attenuation is given by $20\times\log_{10}|S_{21}|$.

III. Calculation for SiO_2 on Si

For ease of calculation and modeling, the complete calculations of Z_0 and the attenuation were performed on an electronic spreadsheet program which had integrated graphics. This integration made it very convenient to test a value for a parameter, compare the resulting calculation of the attenuation for example with the measured value, and then quickly try another value.

IV. Experimental Results

An automatic network analyzer was used to make measurements on a microstrip line structure consisting of silicon dioxide on silicon. The parameters of the structure were estimated before being measured using dimensional and conductivity measurements together with published values for the permittivity and permeability of both dielectric layers. This estimation process resulted in the following values:

$$\sigma_{Au} = 4.6\times10^7\ \text{S/m}$$
$$\epsilon_1 = 4.0$$
$$\epsilon_2 = 11.7$$
$$\sigma_2 = 34.5\ \text{S/m}$$
$$\sigma_1 = 0$$
$$d_1 = 15\ \mu\text{m}$$
$$d_2 = 300\ \mu\text{m}$$
$$w = 90\ \mu\text{m}$$
$$T = 7\ \mu\text{m}$$
$$l = 5.04\ \text{cm}.$$

The frequency range of the measurements was 90 MHz to 18 GHz and a windowing algorithm was used. This algorithm consisted of transforming the data to the time domain, deleting the data that corresponded to parts of the circuit not in the microstrip line itself, and retransforming back to the frequency domain. In other words only data in the time domain window that corresponded to the spatial location of the microstrip line were used. This had the effect of gating out all the reflections in the connectors to the microstrip line and in the transitions from coax to waveguide. The application of this windowing algorithm and the large number of data points (200) resulted in a smooth variation of the actual experimental data plotted in Fig. 3. The windowing algorithm also may have contributed some smoothing.

The various parameters in the model, L, C_1, C_2, G_2, and R, were adjusted, and it was found that the phase of S_{21} and the characteristic impedance were affected to first order only by L and C_1. Referring to the low-frequency approximate relations for Z_0 and $\beta(j\omega)$, the imaginary part of $\gamma(j\omega)$, in [1, eqs. (8) and (9)], we have

$$Z_0 \approx \sqrt{L/C_1} \tag{6}$$

$$\beta(j\omega) \approx \omega\sqrt{LC_1}. \tag{7}$$

The sensitivity experiment confirms that these relations are good approximations over much of the range of the measurements reported here. Therefore a measurement of the magnitudes of Z_0 and $\beta(j\omega)$ by curve fitting allows one to solve (6) and (7) to obtain a unique solution for L and C_1 within this approximation. Having determined these two parameters, it was then possible to determine R from the low-frequency attenuation and G_2 from the slope portion of the curve. The skin effect factor k was multiplied by a constant, less than 1, which was chosen to be such that the proper curvature in the knee of the curve was obtained. It was not possible to determine C_2 from the data since the high-frequency attenuation, where C_2 becomes important, exceeded the dynamic range of the measurement system. In this case, G_1 was taken to be zero since SiO_2 is a very low loss material. We see from Fig. 3 that the phase match is excellent except at the upper frequencies, where the system dynamic range is exceeded. Note that the attenuation match is also quite good.

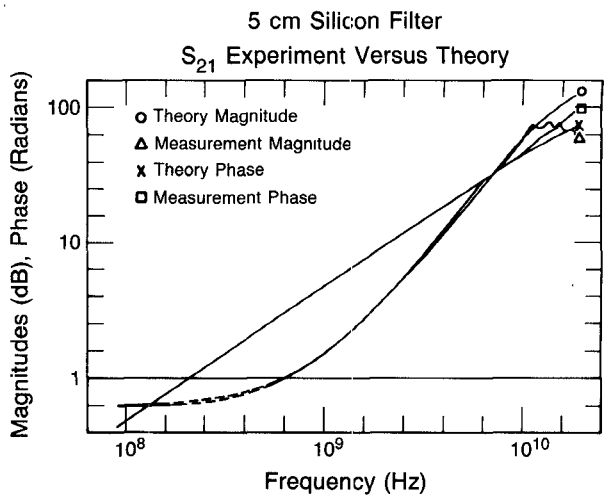

Fig. 3. Measured and modeled attenuation and phase of the microstrip line structure.

TABLE I
Comparison of Values of Parameters Obtained by Fitting Data to Values Obtained by Independent Measurements

Parameter	ANA Measurements	Impedance Measurements
L	711 nH/m	758 nH/m
C_1	306 pF/m	353 pF/m
Z_0	48.2 Ω	48 Ω

The results of the measurement and parameter fitting are given in Fig. 3. In this figure, the logarithm of the attenuation is plotted versus the logarithm of frequency. Since the attenuation is linearly proportional to the propagation constant γ, and γ is proportional to ω^2 in the midfrequency range, the plot should be linear with a slope of 2 in this range if the transfer function, S_{21}, of the microstrip line were Gaussian. In other words, this type of plot enables us to determine the frequency range over which the attenuation is Gaussian-like, which is an important property in network theory. Similarly, the logarithm of phase is plotted versus the logarithm of frequency.

The values of the equivalent circuit parameters obtained by fitting measured data to the model were

$$R = 130\ \Omega/\text{m}$$
$$L = 711\ \text{nH/m}$$
$$C_1 = 306\ \text{pF/m}$$
$$C_2 = 256\ \text{pF/m}$$
$$G_2 = 50\ \text{S/m}$$
$$G_1 = 0.$$

Two of these values together with the characteristic impedance

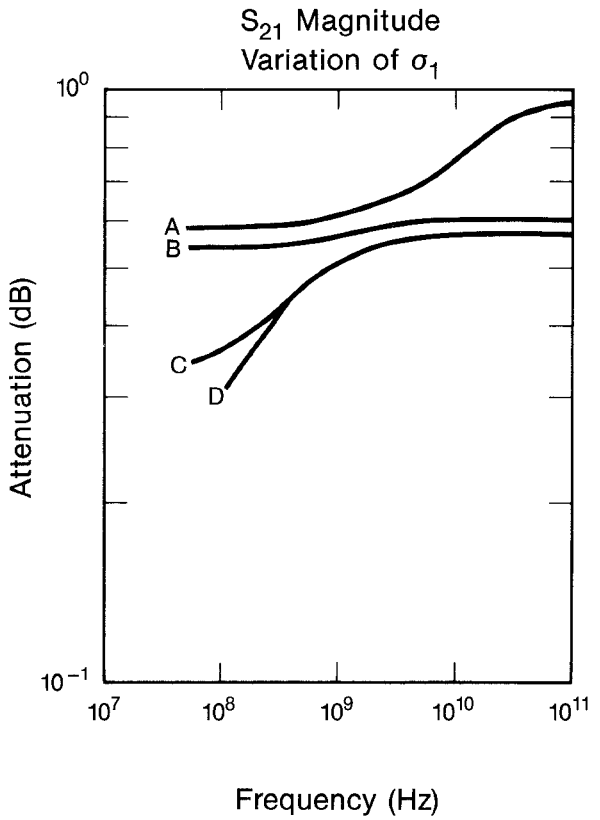

Fig. 4. Attenuation for GaAs on Si microstrip line 1 mm long with $d_1 = 4$ μm, $\sigma_2 = 1.4$ S/m (71 $\Omega \cdot$cm) and A) $\sigma_1 = 10$ S/m (10 $\Omega \cdot$cm), B) $\sigma_1 = 1$ S/m (100 $\Omega \cdot$cm), C) $\sigma_1 = 0.1$ S/m (1000 $\Omega \cdot$cm), and D) $\sigma_1 = 0.002$ S/m ($5 \times 10^4 \Omega \cdot$cm).

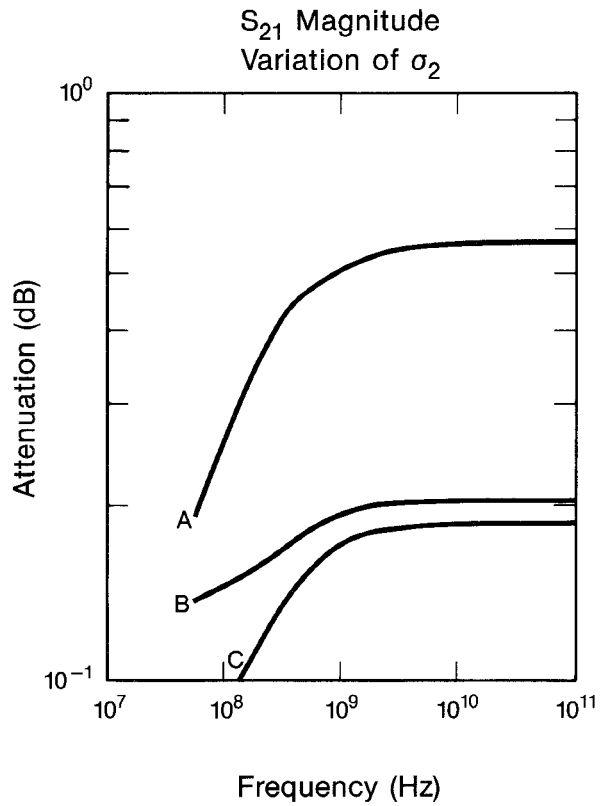

Fig. 5. Calculated attenuation for GaAs on Si microstrip line 1 mm long with $d_1 = 4$ μm, $\sigma_1 = 0.002$ S/m ($5 \times 10^4 \Omega \cdot$cm) and A) $\sigma_2 = 1.4$ S/m (71 $\Omega \cdot$cm), B) $\sigma_2 = 0.1$ S/m (1000 $\Omega \cdot$cm), and C) $\sigma_2 = 0.01$ S/m (10 000 $\Omega \cdot$cm).

were then compared to values obtained by independent short- and open-circuit low-frequency impedance measurements. The result of this comparison is given in Table I.

The good agreement in the determination of Z_0 by the two methods is probably fortuitous since a large error in L can be compensated by a comparable error in C_1 because they occur as a ratio in the expression for Z_0. The discrepancy in the values for L and C_1 between the two methods could correspond to a potential discrepancy in the Z_0 values of 4 percent, which is reasonable for the preliminary measurements reported here.

V. Calculation for GaAs on Si

Having demonstrated the feasibility of determining the equivalent circuit parameters of microstrip lines from measurements, calculations were performed for the important two-layer dielectric case consisting of gallium arsenide on silicon. The purpose of this calculation was to see what range of attenuation to expect using typical dimensions that one might encounter in high-speed integrated circuits. To be consistent with typical materials that can be used for the technology appropriate to GaAs on Si, the following parameters were assumed for these calculations:

$$\sigma_{Au} = 1.5 \times 10^7 \text{ S/m } (6.67 \times 10^{-6} \ \Omega \cdot \text{cm})$$
$$\epsilon_2 = 11.5$$
$$\epsilon_1 = 12.5$$
$$\sigma_1 = 0.002 \text{ to } 10.0 \text{ S/m } (5 \times 10^4 \text{ to } 10 \ \Omega \cdot \text{cm})$$
$$\sigma_2 = 0.01 \text{ to } 1.4 \text{ S/m } (10^4 \text{ to } 71 \ \Omega \cdot \text{cm})$$
$$d_1 = 4 \ \mu\text{m}$$
$$d_2 = 610 \ \mu\text{m}$$
$$w = 10.7 \ \mu\text{m}$$
$$T = 1 \ \mu\text{m}$$
$$l = 1.0 \times 10^{-3} \text{ m}.$$

The calculated attenuation is given in Fig. 4 for one value of σ_2 and four values of σ_1. Fig. 5 gives the attenuation for one value of σ_1 and three values of σ_2. Results are given to 100 GHz; however, above 20 GHz the simple low-frequency model will not give accurate results. Note that the conductivity of the gallium arsenide layer is not zero, as was the case for the silicon dioxide layer.

These curves illustrate the change in behavior of the attenuation versus frequency for various values of σ_1 and σ_2. The width w was chosen to obtain a characteristic impedance of about 50 Ω for $d_1 = 4$ μm and values of σ_2 greater than a few S/m (resistivity less than about 100 $\Omega \cdot$cm). Such values of σ_2 are required to achieve a constant characteristic impedance over a significant range of frequencies. Different values of T also were tried, but the only change was in the low-frequency attenuation, as expected.

These calculations were repeated for $d_1 = 1$ μm, with very little change in the attenuation characteristics. What changes did occur were at the higher frequencies and were not consistent in direction (increase or decrease).

VI. Conclusions

The above results demonstrate the capability to determine the model parameters from network analyzer measurements of structures important to microwave integrated circuits. We have determined that the microstrip line inductance and capacitance of the SiO_2 layer can be uniquely determined by fitting equivalent

circuit parameters to measured data in the frequency range from 90 MHz to 18 GHz. Having demonstrated that this procedure gives reasonable results for the SiO_2 on Si system, we have calculated the attenuation one might expect for GaAs on Si up to a frequency of 100 GHz when fabricating fast integrated circuit devices. However, according to the model used, in the worst case of a low-resistivity Si substrate with a low-resistivity GaAs layer, the loss is less than 1.0 dB/mm out to 100 GHz, which is acceptable for many device applications. Neglecting reflection effects, lower loss circuits could be fabricated using high-resistivity ($10^4\ \Omega\cdot$cm) Si substrates with high resistivity ($5\times10^4\ \Omega\cdot$cm) GaAs layers, where the loss was found to be less than 0.2 dB/mm from 1 to 100 GHz.

References

[1] R. A. Lawton, N. S Nahman, and J. M. Bigelow, "A solid state reference waveform standard," *IEEE Trans. Instrum. Meas*, vol. IM-33, no. 3, pp. 201–205, Sept. 1984.

[2] J. P. Salerno, "Epitaxial growth of GaAs on silicon for integrated circuit applications," in *Proc. 1986 Producibility Millimeter Wave/Microwave Integrated Circuits Conf.* (Huntsville, AL), Nov. 4–5, 1986, p. 21.

[3] H. K. Choi, B. Y. Tsaur, G. M. Metze, G. W. Turner, and J. C. C. Fan, "GaAs MESFET's fabricated on monolithic GaAs Si substrates," *IEEE Electron Device Lett.*, vol. EDL-5, pp. 207–208, June 1984.

[4] H. Morkoc, C. K. Peng, T. Henderson, W. Kopp, R. Fischer, L P Erickson, M. D. Longerbone, and R. C. Youngman, "High-quality GaAs MESFET's grown on silicon substrates by molecular-beam epitaxy," *IEEE Electron Device Lett.*, vol. EDL-6, pp. 381–383, July 1985.

[5] R. Fischer, N. Chand, W. Kopp, H. Morkoc, L. P. Erickson, and R. Youngman, "GaAs bipolar transistors grown on (100) Si substrates by molecular beam epitaxy," *Appl. Phys. Lett.*, vol. 47, no. 4, pp. 397–399, Aug 15, 1985.

[6] A. Christou, B. R. Wilkins, and W. F. Tseng, "Low-temperature epitaxial growth of GaAs on (100) silicon substrates," *Electron. Lett.*, vol. 21, no. 9, pp. 406–408, Apr. 25, 1985.

[7] T. Ishida, T. Nonaka, C. Yamagishi, Y. Kawarada, Y Swano, M. Akiyama, and K. Kamnishi, "GaAs MESFET ring oscillator on Si substrate," *IEEE Trans. Electron Devices*, vol. ED-32, pp. 1037–1041, June 1985.

[8] H. Hasegawa, M. Furukawa, and Y. Hisayoshi, "Properties of microstrip line on Si–SiO_2 system," *IEEE Trans. Microwave Theory Tech.*, vol. MTT-19, pp. 869–881, Nov. 1971.

[9] V. M. Hietala, Y. R. Kwon, and K. S. Champlin, "Low-loss slow-wave propagation along a microstructure transmission line on a silicon surface," *Electron. Lett.*, vol. 22, no 14, pp. 755–756, July 3, 1986.

[10] H. Hasegawa and S. Seki, "Analysis of interconnection delay on very high-speed LSI/VLSI chips using an MIS microstrip line model," *IEEE Trans. Electron Devices*, vol. ED-31, pp. 1954–1960, Dec. 1984.

[11] Y. Fukuoka, Y. Shih, and T. Itoh, "Analysis of slow-wave coplanar waveguide for monolithic integrated circuits," *IEEE Trans. Microwave Theory Tech.*, vol. MTT-31, pp. 567–573, July 1983.

p-i-n Diode Attenuator with Small Phase Shift

ROBERT J. BAETEN, MEMBER, IEEE, T. KORYU ISHII, SENIOR MEMBER, IEEE, AND JAMES S. HYDE

***Abstract*—A computer-aided design technique for minimizing spurious phase shift in microstrip p-i-n diode attenuators is presented. At 9 GHz, a spurious phase shift of 0.17°/dB attenuation has been realized at 15 dB attenuation. This is better than the previous reported value of 1°/dB attenuation at comparable operating frequencies and attenuations. The diode mounting location and the dc blocking chip capacitors on microstrip are important, among other parameters, to minimize the spurious phase shift.**

Manuscript received July 9, 1987; revised October 23, 1987. This work was supported in part by the National Institute of Health under Grants GM27665 and RR01008.

R. J. Baeten was with the Department of Electrical Engineering and Computer Science, Marquette University, Milwaukee, WI. He is now with Rockwell International, Cedar Rapids, IA.

T. K. Ishii is with the Department of Electrical Engineering and Computer Science, Marquette University, Milwaukee, WI 53233.

J. S. Hyde is with the Department of Electrical Engineering and Computer Science, Marquette University, Milwaukee, WI. He is also with the Medical College of Wisconsin, Milwaukee, WI.

IEEE Log Number 8719444.

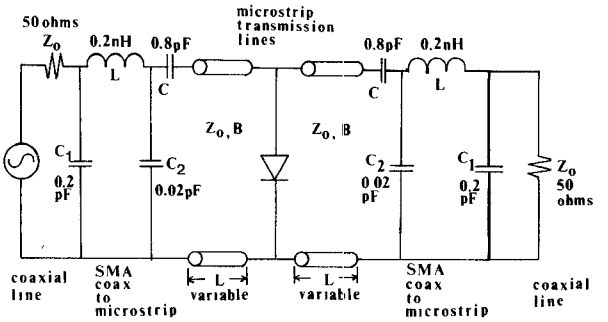

Fig. 1. Minimum parasitic packaged p-i-n diode and two chip capacitors separated by a lossless transmission line.

I. Introduction

Generally, p-i-n diode attenuators have a larger spurious phase shift than waveguide rotary vane type variable attenuators. For example, to the authors' knowledge to date, the best published spurious phase shift for the p-i-n diode attenuators is about 1°/dB attenuation at 9 GHz [1]. On the other hand, for the rotary vane type attenuators, it is 0.1°/dB attenuation [2].

When compact and lightweight features are required, microstrip p-i-n diode attenuators are preferred over bulky and heavy waveguide rotary vane type attenuators. This paper presents a CAD approach to minimize the spurious phase shift in p-i-n diode attenuators.

II. General Circuit Configuration

The general circuit configuration of a single p-i-n diode microstrip attenuator considered in this study is shown in Fig. 1. In this study, an operating frequency of approximately 9 GHz was chosen. All components were chosen from commercially available parts. In this frequency range, chip capacitors [3], p-i-n diodes [4], the printed circuit board, and coax-to-microstrip connectors [5] are commercial components. After selecting these components, the design work reduces to the determination of the characteristic impedance Z_0, the phase constant β, and the length L of the microstrip line to minimize spurious phase shift.

The coax-to-microstrip transition selected was an SMA type 50 Ω connector #50-645-4547-31. The p-i-n diode selected is an Alpha CSB-7401-01 Package #375 [8]. The printed circuit board is RT Duroid 6010.2 Ceramic–PFTE composite laminate ($\epsilon_r = 10.2$, $h = 0.635$ mm, $t = 0.036$ mm, and $\tan\delta = 0.002$). Since this is a 50 Ω system, the characteristic impedance of the microstrip, Z_0, is chosen to be 50 Ω. The blocking chip capacitor is chosen to be 0.8 pF for calculation.

III. Calculation of Attenuation and Phase Shift

The attenuation and phase shift of the p-i-n diode attenuator circuit as shown in Fig. 1 can be calculated using *ABCD* matrices [6], [7]. The overall matrix is calculated from multiplication of *ABCD* matrices of each subsection which include the signal source impedance, the coax-to-microstrip transition sections, the blocking capacitor sections, microstrip line sections, the p-i-n diode mount section, and the load impedance section. This overall matrix can be related to a well-known *s* matrix [6]. Thus